Magnetic Interactions in Dimeric Transition Metal Complexes: Basic *erythro*-Chromium(III)

Sonia Flores

Department of Chemistry, University of Salta, Salta, Argentina

D. E. Ellis*

Department of Chemistry and Materials Research Center, Northwestern University, Evanston, Illinois 60208

Received September 1, 1998

First principles density functional theory is utilized to describe electronic structure and magnetic interactions between Cr(III) ions in linear and bent geometry of [*cis*-[hydroxotetramminechromium-μ-hydroxopentammine-chromium]$^{4+}$. The effective exchange parameter J is extracted and compared with empirical values fitted to experimental data. The calculated value $J = 48$ K for bent geometry compares well with the 30 K experimental value; the magnetic interaction is an order of magnitude larger in the linear configuration. Low-lying optical transitions are analyzed, making use of the transition state scheme, and are in semiquantitative agreement with experimental absorption.

I. Introduction

The well-known *rhodo*- and *erythro*-chromium(III) dimers, first reported by Jørgensen in 1882, have been the subject of intense magnetic and spectroscopic studies.[1] It has been shown by crystallographic methods that the weakly paramagnetic basic rhodo complex contains a linear Cr−O−Cr linkage while the acid rhodo complex contains a bent Cr−OH−Cr unit.[2] The names *rhodo*- and *erythro*- derive from the intense blue and red colors of the complexes in solution. Later convention has identified the rhodo series with a 10:2 ratio of NH_3 ligand to Cr atom and a 9:2 ratio to erythro, of which basic complexes of charge 4+ and acid complexes of charge 5+ have been thoroughly characterized.

The magnetic properties of dimeric transition metal complexes have been shown to be dependent upon their structure, with interest focused upon distance- and angle-dependence of the effective Heisenberg exchange parameter J.[3] Most studies have been based upon fits to experimental susceptibility data using effective Hamiltonians of the Heisenberg type and their generalizations; fits to temperature dependence have been used to test for more elaborate interactions. The present work studies the electronic ground and excited states of linear and bent basic erythro dimers, using the first principles density functional (DF) theory. The resulting orbitals are used to explore magnetic interactions between the Cr ions and low-lying optical transitions of these classic magnetic complexes.

On the basis of fits to magnetic susceptibility, it has been concluded that each Cr ion is in the high spin d^3 ($S = {}^3/_2$) configuration; in an octahedral crystal field, each ion would then have the ground configuration $(t_{2g}{}^{\uparrow})^3\ {}^4T_{2g}$, where the orbital superscripts ($\uparrow$, $\downarrow$) will refer to majority and minority spin, respectively. In the linear conformation of the dimer, the idealized O_h cubic symmetry about the metal is replaced by the 4-fold D_4 symmetry group, and considerable discussion has been made about the possibility of strong metal $M_\pi-L_\pi-M_\pi$ interactions (M = metal, L = ligand). These interactions have been considered responsible for the anomalously low magnetic moment per ion of the linear dimers. The ${}^4T_{2g} \rightarrow ({}^4B_2, {}^4E)$ tetragonal splitting has been associated with IR absorption bands. Bending of the Cr−L−Cr bond would be expected to reduce the coupling, and indeed the moment per atom is observed to increase in the bent complexes. In all cases, the spin-opposed antiferromagnetic Cr−Cr coupling is indicated.

Dunitz and Orgel developed a qualitative molecular orbital model[4] of the linear M−O−M structure, in which $d_{xy,xz}-p_{x,y}$ metal−ligand interactions dominate. The resulting bonding e_u and antibonding e_u* orbitals are of paramount importance, and the remaining symmetry-derived states, e_g, b_{1u}, and b_{2g} play a passive role. More recently, Fink et al. have carried out *ab initio* calculations on linear $L_5M-O-ML_5$ complexes, where M = Ti(III), V(III), Cr(III), and L is an artificial pseudo-He ligand.[5] This important work verified general features of the Dunitz−Orgel model, and permitted for the first time, quantitative estimates of the superexchange coupling between metals, and the resulting magnetic energies. The calculated value of J was found to be notably smaller than experiment for Cr(III), even after extensive configuration interaction and dynamic correlation corrections. One of the possible causes of the discrepancy in magnetic interaction strength is the use of

(1) (a) Jorgensen, S. M. *J. Prakt. Chem.* **1882**, *25*, 321 and 398. (b) Pedersen, E. *Acta Chem. Scand.* **1972**, *26*, 333. (c) Andersen, P. *Coord. Chem. Rev.* **1989**, *94*, 47.

(2) (a) Yevitz, M.; Stanko, J. A. *J. Am. Chem. Soc.* **1971**, *93*, 1512. (b) Urushiyama, A.; Namura, T.; Nakahara, U. *Bull. Chem. Soc. Jpn.* **1970**, *43*, 3971. (c) Cline S. J.; Glerup, J.; Hodgson, D. J.; Jensen, G. S; Pedersen, E. *Inorg. Chem.* **1981**, *20*, 2229. (d) Hodgson, D. J.; Pedersen, E. *Inorg. Chem.* **1980**, *19*, 3116.

(3) Glerup, J.; Hodgson, D. J.; Pedersen, E. *Acta Chem. Scand.* **1983**, *A37*, 161 and references therein.

(4) Dunitz, J. D.; Orgel, L E. *J. Chem. Soc.* **1953**, 2594.

(5) Fink, K.; Fink, R.; Staemmler, V. *Inorg. Chem.* **1994**, *33*, 6219.

10.1021/ic981049x CCC: $15.00
Published on Web 11/12/1998

artificial ligands, with some concomitant distortion of the M−O−M bonding structure. One of the goals of the present work is to give a more detailed analysis of metal−ligand interactions.

II. Computational Details

The Discrete Variational (DV) method, which is extensively described in the literature,[6] has been employed in the calculations. In the present implementation of the variational approach, the one-electron molecular wave functions are expanded as a linear combination of numerical atomic orbitals (LCAO). Matrix elements of the DF Hamiltonian and overlap are calculated by numerical sampling/integration, and a standard secular matrix equation is solved to obtain the expansion coefficients. The LCAO basis is optimized in the sense that the self-consistent Mulliken AO populations are used iteratively to generate the basis. The von Barth−Hedin version of the exchange-correlation potential[7] was used; the results are not expected to be very sensitive to this aspect of potential approximation. Tests made with the Vosko−Wilk−Nusair variant[8a] of V_{xc} confirm this expectation. Gradient corrections to the exchange-correlation energy are commonly applied, to improve the absolute binding energy and bond lengths;[8b,c] these corrections are most conveniently applied outside the self-consistent-field (SCF) procedure. In the present *differential* magnetic transition state calculations (see below) the relevant energies are calculated within the SCF iterations, and gradient corrections are believed to be unnecessary. In any case, they are beyond the scope of the present work.

With covalent bonding between metal and ligands essentially controlling the long-range magnetic interactions, it is most important to obtain a good representation of the molecular charge density and Coulomb potential. To obtain a good representation we have used a least-squares variational fit to the density, in the so-called self-consistent multipolar scheme.[9]

In the calculations both the bond lengths and bond angles in the basic *cis*-$[(NH_3)_5Cr(OH)Cr(NH_3)_4(OH)]^{4+}$ ion were fixed so as to obtain the average values reported for the crystal structure.[2d] The existence of a complete structural and magnetic characterization of the basic erythro complex was a motivation for studying this particular complex. A view of the bent cation, with Cr−O−Cr angle of 143° and bond lengths Cr(1)−O(1) and Cr(2)−O(1) of 1.96 and 1.99 Å, respectively, is given in Figure 1. The idealized linear structure was simply obtained by opening the Cr−O−Cr angle to 180° while maintaining other bond angles and lengths constant. This will permit a close comparison of geometry-dependent results, which would not be possible if experimentally known linear systems like $[\{Cr(NH_3)_5\}_2O]$ [2a] or $[\{Cr(NCS)(TPyEA)\}_2O]$,[10] which have both structural and chemical differences, were substituted. The bond lengths and bond angles of the two complexes studied are given in Tables 1 and 2. In the linear model system, the Cr(1)−O(1)−H angle was maintained at 87°, the same as in the experimental bent system.

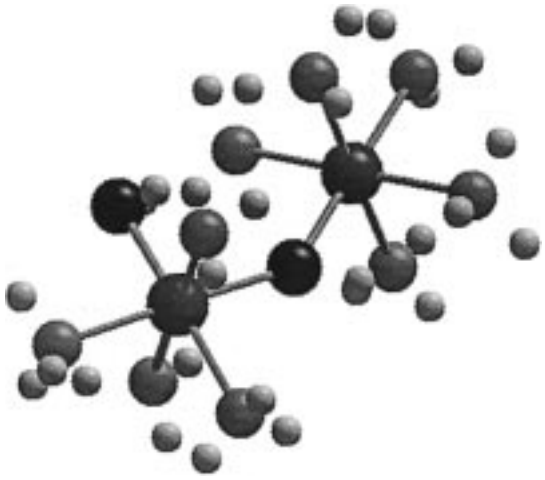

Figure 1. Schematic view of experimental *cis*-$[(NH_3)_5Cr(OH)(NH_3)_4(OH)]^{4+}$ structure used in calculations.

Table 1. Interatomic Distances (Å) in Basic Erythro Linear and Bent Cr(III) Dimers (from Ref 2d)

	distance	
atoms	linear	bent
Cr(1)−Cr(2)	3.926	3.744
−O(1)	1.963	1.962
−N(1)	2.062	2.111
−N(2)	2.066	2.079
−N(3)	2.102	2.102
−N(4)	2.107	2.107
−N(5)	2.110	2.062
Cr(2)−O(1)	1.963	1.989
−O(2)	1.914	1.915
−N(6)	2.098	2.097
−N(7)	2.054	2.055
−N(8)	2.075	2.075
−N(9)	2.090	2.090
O(1)−H(1)	1.097	1.10
O(2)−H(2)	0.926	0.926

Table 2. Selected Bond Angles (deg) of Basic-Erythro Cr(III) Dimer (from Ref 2d)

atoms	angle	atoms	angle
Cr(1)−O(1)−Cr(2)	142.8	O(1)−Cr(2)−O(2)	91.6
O(1)−Cr(1)−N(1)	178.9	−N(6)	89.1
−N(2)	91.2	−N(7)	90.4
−N(3)	91.3	−N(8)	91.1
−N(4)	91.2	−N(9)	178.8
−N(5)	89.6	O(2)−Cr(2)−N(6)	178.8
N(1)−Cr(1)−N(2)	88.7	−N(7)	90.3
−N(3)	89.8	−N(8)	93.0
−N(4)	88.9	−N(9)	89.5
−N(5)	89.3	N(6)−Cr(2)−N(7)	88.7
N(2)−Cr(1)−N(3)	89.7	−N(8)	88.0
−N(4)	177.4	−N(9)	89.8
−N(5)	91.6	N(7)−Cr(2)−N(8)	176.3
N(3)−Cr(1)−N(4)	91.2	−N(9)	89.7
−N(5)	178.3	N(8)−Cr(2)−N(9)	88.7
N(4)−Cr(1)−N(5)	87.4		

The geometry around the two independent chromium(III) sites is roughly octahedral, and for the linear dimer the symmetry is roughly D_4. These approximate symmetries are very useful for construction of qualitative models and analysis of numerical results. However, for the sake of numerical accuracy, we have carried out all calculations in C_1 symmetry, that is, with no symmetry elements. For the Cr(1) ion the ligating atoms are the oxygen O(1) of the bridging hydroxyl group and the five

(6) (a) Ellis, D. E.; Painter, G. S. *Phys.Rev.* **1970**, *B2*, 2887. (b) Baerends, E. J.; Ellis, D. E.; Ros, P. *Chem. Phys.* **1973**, *2*, 41. (c) Rosen, A.; Ellis, D. E.; Adachi, H.; Averill, F. W. *J. Chem. Phys.* **1976**, *65*, 3629; (d) Ellis, D. E; Guo, J. In *Density Functional Theory of Molecules, Clusters, and Solids*; Ellis, D. E., Ed.; Kluwer: Dordrecht, 1995; p 263.
(7) von Barth, U.; Hedin, L. *J. Phys.* **1972**, *C5*, 1629.
(8) (a) Vosko, S. H.; Wilk, L.; Nusair, M. *Can. J. Phys.* **1980**, *58*, 1200. (b) Becke, A. D. *Phys. Rev.* **1988**, *A38*, 3098. (c) Perdew, J. P. *Phys. Rev.* **1986**, *B33*, 8622; **1986**, *B34*, 7046.
(9) Delley, B.; Ellis, D. E. *J. Chem. Phys.* **1982**, *76*, 1949.
(10) Di Vaira, M.; Mani, F. *Inorg.Chem.* **1984**, *23*, 409.

Table 3. Self-Consistent Mulliken Atomic Orbital Populations for Basic Erythro Linear and Bent Cr(III) Complexes in Their Ground State

		linear		bent				linear		bent	
orbital		charge	spin	charge	spin	orbital		charge	spin	charge	spim
Cr(1)	3d	3.824	3.147	3.803	3.275	N(2)	2s	1.143	0.015	1.163	0.018
	4s	0.045	0.006	0.036	0.011		2p	4.062	0.066	4.081	0.081
	4p	0.118	0.017	0.113	0.022		3s	0.124	−0.005	0.120	−0.007
total		2.013	3.170	2.048	3.308		3p	0.207	−0.013	0.191	−0.012
						total		−0.537	0.063	−0.555	0.082
Cr(2)	3d	3.822	−3.101	3.807	−3.207						
	4s	0.027	−0.004	0.019	−0.004						
	4p	0.122	−0.026	0.088	−0.013						
total		2.028	−3.131	2.085	−3.224						
O(1)	2s	1.842	0.005	1.805	0.002	N(3)	2s	1.157	−0.016	1.162	−0.022
	2p	4.846	−0.011	5.196	−0.003		2p	4.030	−0.075	4.026	−0.101
	3s	0.073	0.005	0.071	0.000		3s	0.122	0.003	0.125	0.005
	3p	0.228	0.003	0.164	−0.001		3p	0.202	0.014	0.204	0.013
total		−0.988	0.002	−1.236	−0.002	total		−0.511	−0.074	−0.517	−0.105
O(2)	2s	1.719	−0.007	1.734	0.003	N(4)	2s	1.095	0.015	1.095	0.022
	2p	4.856	0.099	4.993	0.052		2p	3.954	0.069	3.945	0.101
	3s	0.131	−0.010	0.110	−0.005		3s	0.120	−0.004	0.125	−0.005
	3p	0.122	−0.002	0.080	−0.005		3p	0.202	−0.012	0.208	−0.010
total		−0.828	0.080	−0.918	0.045	total		−0.372	0.068	−0.373	0.108
N(1)	2s	1.108	−0.007	1.120	−0.008	H(1)	1s	0.908	0.006	0.671	−0.007
	2p	4.088	−0.032	4.029	−0.037	total		0.092	0.006	0.329	−0.007
	3s	0.124	0.001	0.123	0.002	H(2)	1s	0.726	−0.003	0.774	−0.005
	3p	0.204	0.003	0.199	0.005	total		0.274	−0.003	0.226	−0.005
total		−0.524	−0.035	−0.472	−0.038	H(3)	1s	0.779	0.001	0.787	0.001
						total		0.221	0.001	0.213	0.001

ammine nitrogen atoms; while for the Cr(2) ion one ammonia ligand has been substituted by the terminal hydroxyl oxygen O(2).

III. Calculations and Results

A. Ground State. A.1. Linear Case. The self-consistent Mulliken atomic orbital populations for charge and spin are given for the antiferromagnetically coupled ground state in Table 3. We see that the spin-polarized DV calculations verify the high-spin Cr(III) configuration suggested from fits to magnetic susceptibility. We note that the net Cr ionic charge is close to 2, less than the nominal value of 3, due primarily to the presence of considerable metal d−oxygen p covalency, contributing 0.82 e. A small but nonnegligible diffuse Cr 4s,4p component accounts for the remainder. For the ground state both the lowest unoccupied and highest occupied electronic energy levels are shown in Table 4, together with selected Mulliken atomic orbital populations. In addition to localization driven by spin-exchange, the eigenvectors are localized into different parts of the molecule due to the somewhat different chemical environment of the two cations. The spin polarization results in an intra-atomic exchange splitting of ∼3.0 eV between the spin-up and spin-down levels which are predominantly of Cr 3d character, on a particular site. The average spin moment is 3.15 μ_B, slightly larger than in the isolated free ion. The largest induced spin moment on the ligands is ∼0.08 μ_B, associated with O(2). In the inversion-symmetric linear case, the net moment on O(1) would be zero by symmetry, so the perturbation by substitution of one hydroxy for ammine ligand has little effect on the O(1) spin. A significant polarization of 0.04−0.07 μ_B is also predicted on the nitrogen sites.

Densities of states (DOS) diagrams for the charge and spin distribution are given in Figure 2. With a large number of valence MOs, DOS offers a convenient means of analyzing distribution of energy levels. The partial DOS of Cr(1) 3d and Cr(2) 3d, as well as the bridging oxygen O(1) sp states are given separately, to emphasize their contributions. In addition to the well defined ligand-field and exchange-split Cr 3d peaks, one can see the diffuse 3d−O 2p bonding hybridization extending across the upper valence band. The spin-DOS clearly defines the opposing 3d Cr(1) ↑, Cr(2) ↓ characteristics, essentially degenerate, in the occupied region and a double-peak structure in the vacant region. The alternating polarization on O(1), which averages to ∼zero, is seen to be significant in individual levels.

Table 4. Lowest Unoccupied and Highest Occupied Energy Levels(eV) for Ground State of the Linear Basic Erythro Complex, with Selected Mulliken Atomic Orbital Populations (%); Symbols (+) and (−) Indicate Up and Down Spin, Respectively, and Level 47− is the Highest Occupied Molecular Orbital

		Cr(1)	Cr(2)	O(1)	O(2)	N(1)	N(2)	N(3)	N(4)	H(1)
level	energy	3d	3d	2p	2p	2p	2p	2p	2p	1s
52+	−17.50		90		4	1				
51−	−17.61	90	1	4		1				
51+	−17.62	63	1			30				
50+	−17.68	5	77	4		1		1	1	
50−	−17.74	89	2			1				
49+	−17.78	3	82	3		1				
49−	−17.85	93	1			1				
48+	−17.93	55	16	3		10		9		
48−	−17.99	6	60	5	2	4	5		9	
E_F										
47−	−19.82	1	49	2	37	1				3
47+	−19.88	32	2	9	38	1				5
46−	−20.18	1	86	4					1	
45−	−20.33	1	75	5	10	1				1
46+	−20.36	89	1	1	2	1				
45+	−20.55	95								
44−	−20.56	1	62	3	20	1			1	2
44+	−20.73	66	1	2	24					1
43+	−22.35	2	5	7	80	2				
43−	−22.53		13	9	69	3			1	
42−	−23.98	5		2	1	81		6		
42+	−24.19	6	1	8	2	70	2	3	2	
41−	−24.26			3	1	87		1		

Contour maps of charge and spin density are given in Figure 3, in the plane containing both Cr, O(1), and the terminal oxygen O(2). The extensive covalent mixing between metal and ligand is very evident in the charge figure, and the antiferromagnetic

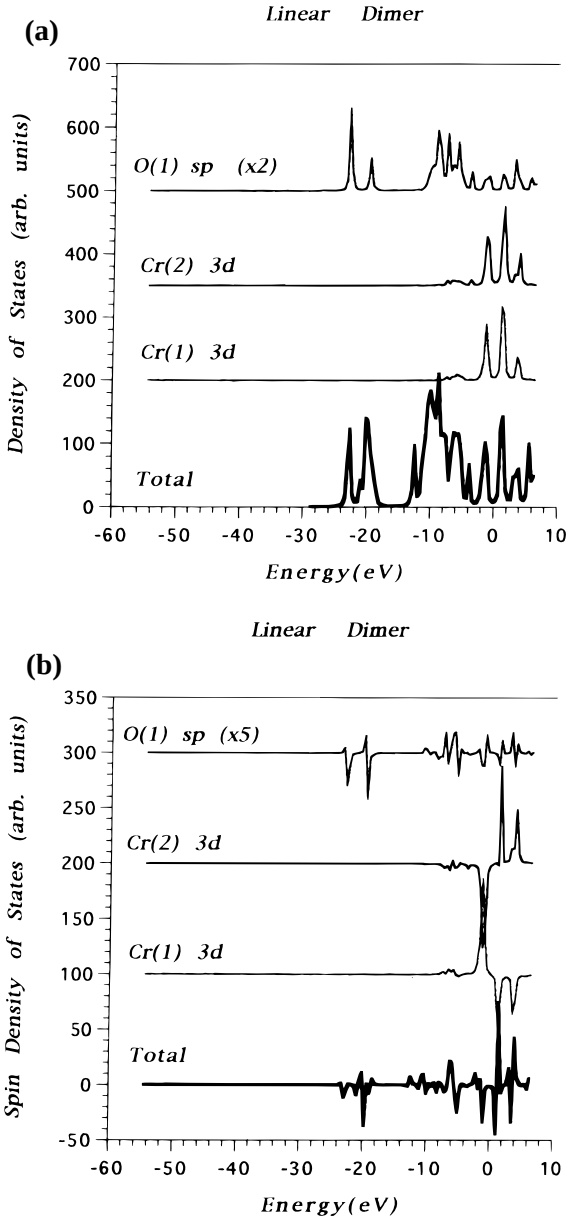

Figure 2. Densities of states (DOS) diagrams for the (a) charge and (b) spin distribution of the linear dimer. The zero of energy is the Fermi energy E_F, halfway between HOMO and LUMO.

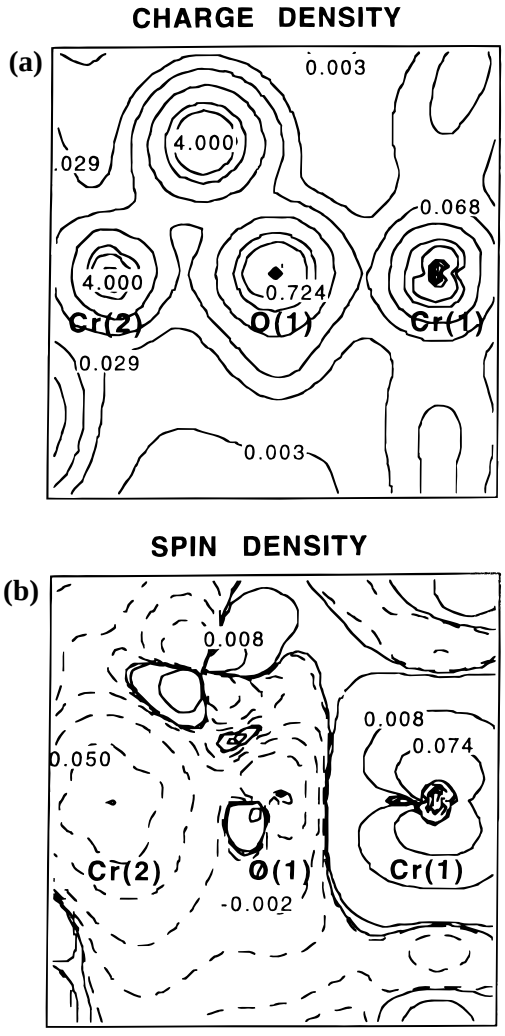

Figure 3. Contour maps of (a) charge and (b) spin density , in the plane containing both Cr, O(1) and the terminal oxygen O(2), for the linear dimer. Contour spacing is not uniform, key values are identified.

ground state spin order is seen in the spin map. In addition to the expected Cr−O(1) covalent bonding charge, we can also see a significant O(1)−O(2) shared charge. The spin density map shows a strongly polarized O(2), despite its "terminal" position. We can predict that the cis and trans isomers will differ significantly in this respect. The HOMO and LUMO are shown in Figure 4, in the same plane as for previous maps, revealing important nodal surfaces and charge distribution. As it would be very tedious to list all significant atomic orbital components of the molecular orbitals which contribute to magnetic and optical properties, graphical methods seem more appropriate. The HOMO is dominated by Cr(2) 3d character; it shows an interesting mixture of π- and σ-bonding toward O(1), with the bond charge maximum canted ~45° with respect to the Cr(2)−O(1) bond axis. The Cr(2)−O(2) bond character in this orbital is more nearly of σ-type, but curiously built up from a d_{xz} lobe and O sp-hybrid character. The LUMO, being dominated by Cr(1) 3d, has equally interesting nodal character, showing a larger O(2) p character with a bond-line (in the topological sense) bent away from the Cr(2)−O(2) axis. The LUMO is antibonding with respect to the O(1)−O(2) axis, and an extended π-overlap region is seen to couple Cr(1), O(1), and Cr(2).

A.2. Bent Case. The charge and spin populations of Table 3 for the experimentally realized bent case show a metal configuration similar to that of the linear structure. The most striking difference is the greater ionicity of both bridging and terminal oxygens, which is compensated by lesser charge on the ammine groups. The most important occupied and vacant valence levels for the bent structure are listed in Table 5, along with selected atomic populations. The difference in ligation, leading to what we may call "chemical-exchange" splitting, amounts to ~1.3 eV in the case of the center of gravity of the (occupied) majority spin Cr(1) vs Cr(2) 3d levels. The six highest occupied molecular orbitals contain the dominant Cr contributions. From the populations given in Table 3, we verify that the 45, 46, and 47 ↑ and 45, 46, and 47 ↓ levels are localized on Cr(1) and Cr(2), respectively.

In the cis configuration, the ligands of Cr(1)and Cr(2) are located on alternate positions; for this reason one can expect a reduced overlap among the d_{xy}, d_{xz}, and d_{yz} atomic orbitals of both atoms, compared to the linear case. The calculated net spin of 0.012 μ_B of the ground state corresponds in good approximation to a singlet state, with antiferromagnetic sym-

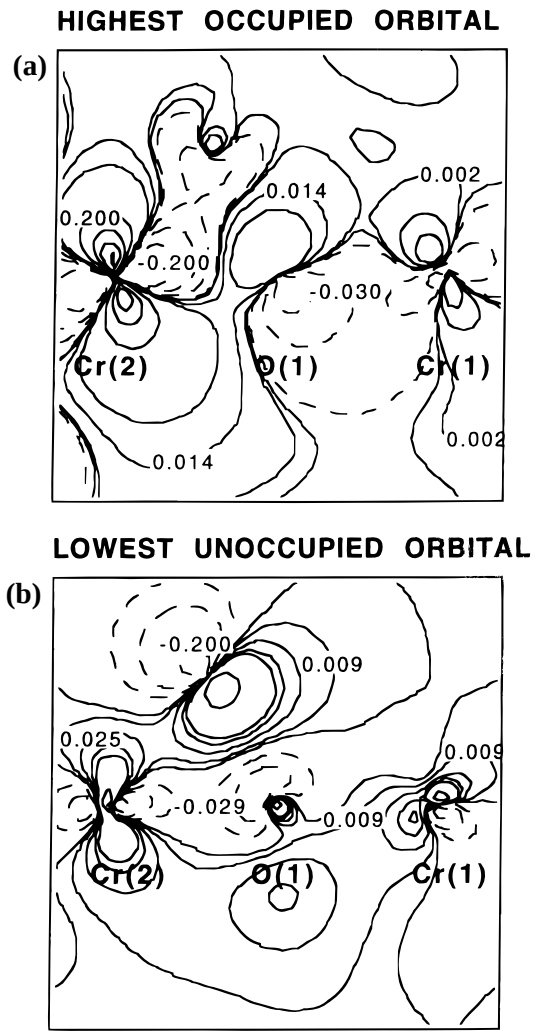

Figure 4. (a) Highest occupied molecular orbital for linear dimer, in same plane as previous map. (b) Lowest unoccupied molecular orbital.

metry. The average Cr moment increases to 3.27 μ_B, a result of the weakened coupling between the ions, and consistent with experiment. The net cancellation of their nearly equal (↑, ↓) moments leads to the observed small net spin. Further evidence of weakened spin coupling is the reduction of the O(2) induced moment to about half of its value in the linear dimer.

Density of states diagrams for charge and spin are given in Figure 5, in the Cr(1)−O(1)−Cr(2) plane. They show a similar degree of covalent charge mixing, and a polarization of the bridging oxygen, as found in the linear case. The Cr 3d three-peak ligand-field plus exchange structure is preserved, as is the 3d−O 2p hybridization across the valence band. The spin DOS now shows the Cr(1) and Cr(2) 3d peaks to lie at slightly different energy, with Cr(1) being more tightly bound. Polarization of O(1) is found to be about one half that of the linear case, again integrating to ∼zero moment.

Contour maps of charge and spin density are given in Figure 6; from the perspective given one can get some impression of Cr(2)−N(1) versus Cr(2)−O(2) bonding charge. The Cr(2)−O(2) bond charge appears to be similar to that of the linear case, despite the indication from atomic populations that O(1) is more ionic here. The spin density map shows that Cr(1) and Cr(2) are indeed nearly equivalent, though inverted in sign. Polarization of the bridging oxygen has a curious angular character, dominated by the antiferromagnetic dipole oriented nearly along the Cr(1)−Cr(2) line. The net magnetic interaction is found to be considerably weaker in the bent configuration, as found experimentally, previously explained on a semiempirical basis, and discussed in detail in the following.

Table 5. Lowest Unoccupied and Highest Occupied Energy Levels (eV) for Ground State of the Bent Basic Erythro Complex, with Selected Mulliken Atomic Orbital Populations (%); Symbols (+) and (−) Indicate Up and Down Spin, Respectively, and Level 47− is the Highest Occupied Molecular Orbital

level	energy	Cr(1) 3d	Cr(2) 3d	O(1) 2p	O(2) 2p	N(1) 2p	N(2) 2p	N(3) 2p	N(4) 2p
50+	−17.71	1	91	2					
50−	−17.86	89	3	3		1			1
49+	−17.97	65	1			28			
49−	−18.10	87	4			1			1
48+	−18.14	58	11	4		11		9	
48−	−18.16	80	9		1	1			2
E_F									
47−	−19.76		75		21				
46−	−20.10		89	1	4				
45−	−20.30	1	92	3	1				
47+	−20.54	90	1	5		1			
46+	−20.73	94		1					
45+	−20.82	93							
44+	−22.04		4	1	88	1	1		1
44−	−22.33		18	1	73	2	1		
43+	−22.56		5		85	4			
43−	−22.83		10	1	77	6	1		
42+	−24.39	1	2	17	3	37	9		24
42−	−24.40	1	4	26	2	44	17	2	
41+	−24.42	1	1	8	1	11	18		51
41−	−24.58	3	1	3	1	72	1	1	13

The HOMO and LUMO maps appear in Figure 7. The HOMO is dominated by Cr(2) 3d character, aligned favorably for bonding with O(1) p_π orbitals. At the same time, Cr(1) d_π−O(1) p_π overlap is seen, as predicted in qualitative models of the key orbital interactions. The LUMO shows itself to be also a complex mixture of d_π and p_π character; although not evident from this view plane, it is dominated by Cr(1) character (see Table 5).

B. Magnetic Transitions. Magnetic interactions in binuclear transition metal complexes have primarily been studied via the temperature-dependent susceptibility χ_M. The effective metal−metal interaction has been conveniently represented in terms of the Heisenberg $J(S_i \cdot S_j)$ Hamiltonian, and possibly other additional bilinear interactions, the spin−dipolar field, Curie-law contributions of impurities, and a temperature-independent conduction electron term. Typical values of J are 10−30 K, in k_BT temperature units, with dimensionless spin. In the present case, the $S = {}^3/_2$ Cr ions can couple to produce states with a total spin of $S_t = 0, 1, 2, 3$. Since the coupling is essentially indirect, through the bridging ligand, and with possibile environmental effects of the remaining terminal ligands, it is by no means clear that a simple bilinear spin-coupling is adequate to describe the magnetic energy level structure. In fact, some workers have preferred to directly fit the magnetic energy levels as parameters in χ_M.[3]

The single-electron energy levels can, as described above, give an approximation to total energy differences via the transition state procedure. One procedure to extract the different S_t state energies would be to perform calculations for M_t values of 0, 1, 2, 3 (here $M_t = \langle S_Z \rangle$, the only good spin quantum number of spin-polarized calculations). We could then use a projection method similar to the Slater sum rule long used in atomic structure calculations to determine the individual state energies. Here we choose a shortcut, focussing only on the extreme case of spin−flip of one Cr ion, to obtain an approximation to the

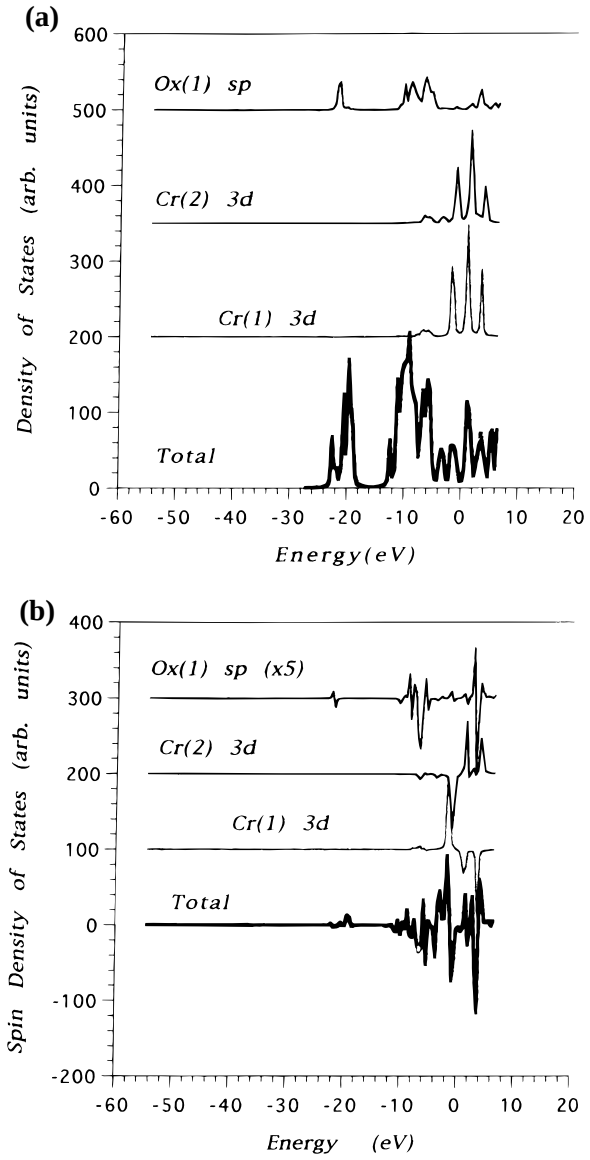

Figure 5. Density of states diagrams for (a) charge and (b) spin for the bent dimer.

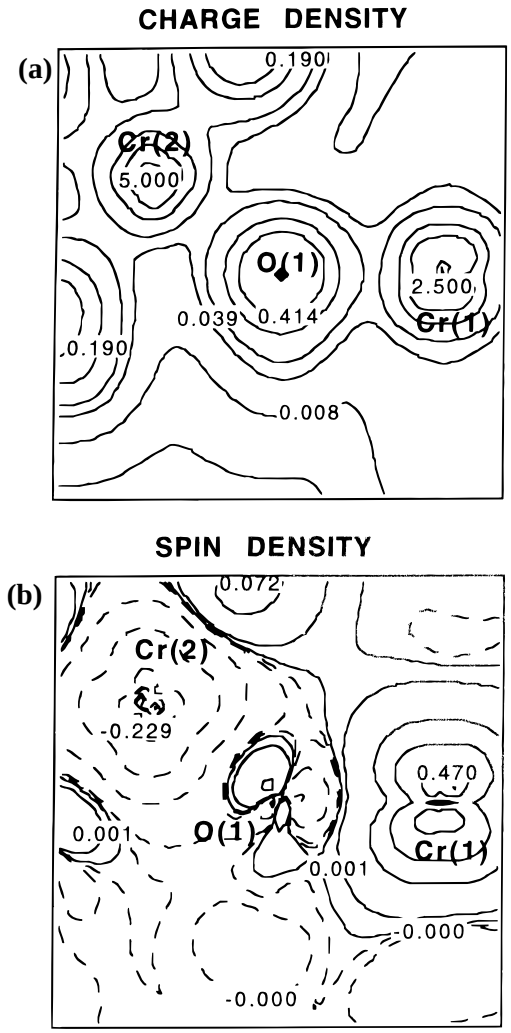

Figure 6. Contour maps of (a) charge and (b) spin density, in the plane containing Cr(1), Cr(2), and O(1) for the bent dimer.

singlet−septet energy difference and hence the desired J parameter for comparison with experiment.

According to Slater's transition state (TS) theory,[11] a good approximation to total energy differences can be obtained by performing SCF calculations in which $^1/_2$ electron is transferred from the initial state to the final state configuration. The general expression for the total energy difference is

$$\Delta E_{\text{tot}} \cong \sum_i \Delta n_i \epsilon_i^* \qquad (1)$$

where Δn are differences in occupation number between initial and final state and ϵ^* are the TS orbital eigenvalues.

In the *magnetic* transition state, where interest is focussed upon spin reversal at a particular site, the internal field due to exchange at the probe site averages to zero. Then the probe-site electrons sample the exchange field due to the neighboring atoms; in this way a very high sensitivity and accuracy is obtained.[12] In the present work, we determine the energy differences of eq 1 due to exchange splitting of MO's localized on Cr(2), in response to the polarization primarily localized on Cr(1) and passed through the ligand bridge. The boundary conditions are easily satisfied by zeroing the spin-polarization on the Cr(2) site in each SCF iteration; the Coulomb potential is not perturbed. In the d^3 ion three MO's are expected to make significant contributions and are easily identified from the partial density of states diagram of the TS levels.

Our calculated values for J, in units of k_BT, are 48 K for the bent dimer and 514 K for the linear case; the experimental value for the bent case is 30 K.[2c] We thus find that, as observed in experiment and explained qualitatively by orbital interaction models discussed above, the linear dimer magnetic interactions are a full order of magnitude stronger than those of the bent dimer. As discussed by Spiccia *et al.*[13] the observed J values apparently depend upon a variety of parameters, among which are M−M distance, M−O bond length, M−O−M bond angle, bridging O−H tilt angle, and crystal packing effects. The semiquantitative agreement between theory and experiment found here is quite satisfactory in view of the relative simplicity

(11) Slater, J. C. *The Self-Consistent Field for Molecules and Solids*; McGraw-Hill: New York, 1974.

(12) (a) Gubanov, V. A.; Ellis, D. E. *Phys. Rev. Lett.* **1980**, *44*, 1633. (b) Guo, L.; Ellis, D. E.; Mundim, K. C.; Hoffman, B. M. *J. Porphyrins Phthalocyanines* **1998**, *2*, 1.

(13) Spiccia, L.; Fallon, G. D.; Markiewicz, A.; Murray, K. S.; Riesen, S. *Inorg. Chem.* **1992**, *31*, 1066.

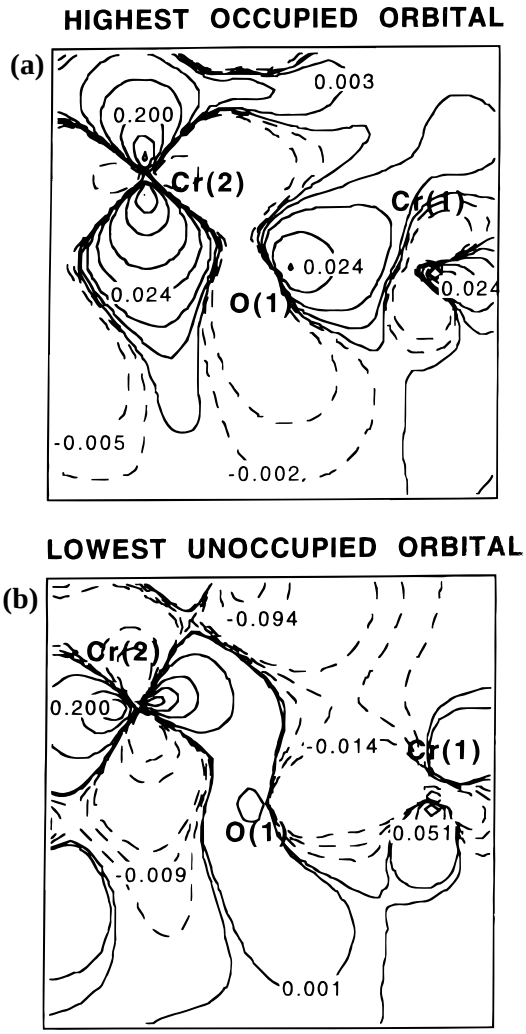

Figure 7. (a) Highest occupied molecular orbital for bent dimer, in same plane as previous map. (b) Lowest unoccupied molecular orbital.

of the isolated molecule density functional model employed. Reasonable variations of metal−μ(OH) angle and M−O distances in the linear model would of course make some quantitative changes in the value of J (linear). However, they would not alter the basic mechanism of strong magnetic interaction brought about by collinear alignment of Cr(1)−O−Cr(2) valence orbitals. The calculated magnetic moments at each site for both linear and bent cases are given in Table 3; the predicted average Cr moment of 3.27 μ_B can be compared with the effective moment $\mu_{eff} = 3.6\ \mu_B$ measured at 300 K. Recall that for the free ion $g\sqrt{s(s+1)} = 3.87$.

In order to understand the superexchange mechanism better, we show bond-line spin maps for the two cases in Figure 8. The polarization wave passing from one metal to the other, through the bridging oxyanion is particularly interesting. As predicted in qualitative MO models, the coupling is calculated to be considerably weaker in the bent case, compared to linear. We see here that the O(1) polarization is *qualitatively* different in the strong-coupled linear case, having considerable s character, while the bent case O(1) density is both smaller and almost entirely of p character.

C. Optical Absorption. There are several cases of interest here.

(1) The usual intense optical transitions are attributed to one-electron dipole allowed processes with no change in spin state. These can be approximately read off the ground state energy

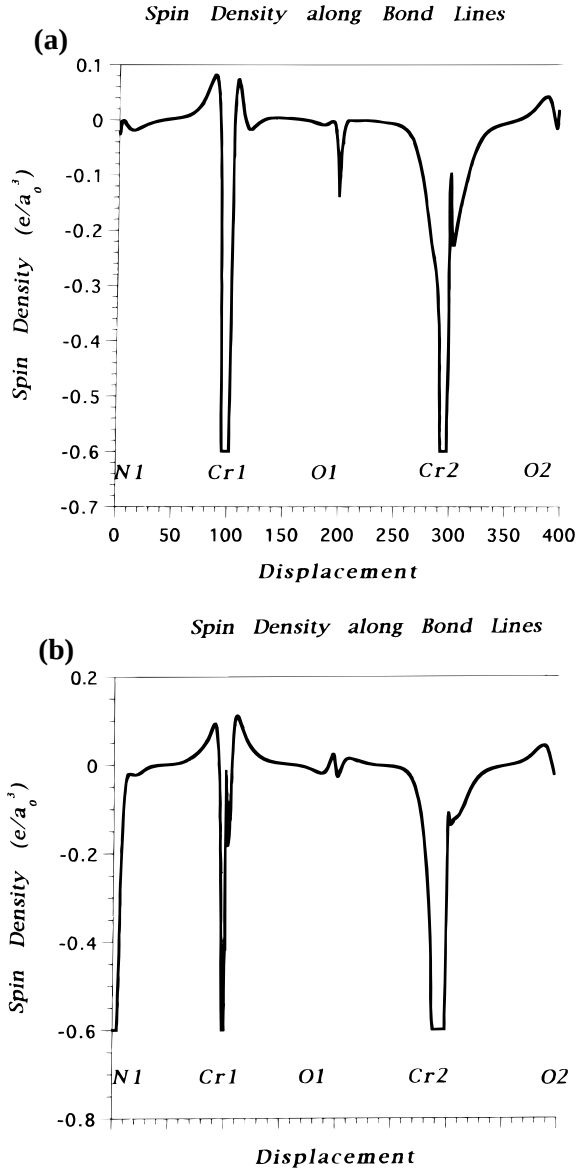

Figure 8. Bond-line spin maps (e/a_0^3) for (a) linear and (b) bent dimer. Large core-polarization values have been truncated to 0.6 e/a_0^3.

level diagram, and more accurately determined through transition state calculations which include electronic final state relaxation. As we have no experimental absorption spectra available for the $[(NH_3)_5Cr(OH)(NH_3)_4(OH)]^{4+}$ cation of the present study, we compare our results with measured spectra for similar complexes; differences among these complexes are not great. Here we cite typical experimental absorption of two dinuclear chromium ammine complexes in the literature, presenting two broad bands between 420−600 and 310−420 nm approximately. The absorption maxima are[14]

(a) *cis*-$[(NH_3)_5Cr(OH)Cr(NH_3)_4(OH)_2]^{5+}$,
510 nm (2.43 eV); 374 nm (3.31 eV)

(b) *cis*-$[(NH_3)_5Cr(OH)Cr(NH_3)_4Cl]^{4+}$,
520 nm (2.38 eV); 380 nm (3.26 eV)

The HOMO(47↓)−LUMO(48↓) energy difference for the ground state of bent *cis*-$[(NH_3)_5Cr(OH)Cr(NH_3)_4(OH)]^{4+}$ is calculated to be 1.60 eV; when the TS calculation is made to include

(14) Hoppenjans, D. W.; Hunt, J. B. *Inorg.Chem.* **1969**, *8*, 505.

electronic relaxation, the result is 2.00 eV. The first band of allowed transitions, built up primarily from d→d transitions made intense by the admixture of ligand character, spans ∼1.5 eV, thus corresponding nicely with the optical bands centered at 2.4 and 3.3 eV. The splitting of ∼0.9 eV between bands is apparently related to the ∼0.8 eV offset between (↑, ↑) and (↓, ↓) spin transitions. As seen from Table 5, the next optical absorption band is predicted to have considerable terminal oxygen character in the initial state 44↑; transitions into the available Cr d levels would thus be of intense charge transfer (CT) nature. Assuming a similar TS shift, the CT band would have an onset at ∼4.3 eV.

(2) We may also consider one electron spin−flip transitions in which a spin-up electron localized in an occupied state on one side of the molecule is excited into a vacant spin-down level on the *same* side of the molecule; e.g., 47↓ → 50↑. This gives a measure of exchange coupling and d-electron correlation on a given Cr site; i.e. intraatomic magnetic energies. From the ground state energy levels, we see that this transition occurs at ≥2.1 eV, and will also fall in the visible region. Presumably these transitions are rather weak and hidden by the spin-allowed bands.

(3) Finally, we may consider transitions like 47↓ → 48↑ where the initial state is localized on Cr(2) and the final state is localized on Cr(1). This corresponds to a net spin change of the complex (from 0.012 to 1.000 μ_B**)** associated approximately with reduction of the Cr(2) moment from 3.22 to 2.51 μ_B. For the spin− and site−flip transition just mentioned, the calculated excitation energy is 2.03 eV, compared with an estimate made from ground state orbital energies of 0.38 eV. Thus, changes in correlation energy with excitation account for most of the net energy difference.

IV. Conclusion

We have calculated the ground state, magnetic structure, and low-lying optical spectra of the *cis-erythro*-Cr(III) dimer, using a first principles density functional approach. The results support previous analyses in terms of qualitative molecular orbital models, and are in semi-quantitative agreement with experiment. Specific details of covalent mixing between metal d and ligand atomic orbitals are determined for the first time. The superexchange mechanism which couples spin of one metal to the other, through the intervening ligand, is made apparent by means of bond-line spin maps and spin-density contour maps.

Acknowledgment. This work was supported by the MRSEC program of the National Science Foundation (DMR-9632472) at the Materials Research Center of Northwestern University, by NSF−INT (Grant. No. INT-9600016), and by the Argentine National Science Foundation. We thank Centro Brasileiro de Pesquisas Fisicas, Rio de Janeiro, for their hospitality and use of facilities during the period in which this work was begun.

IC981049X